X. PLASMA MAGNETOHYDRODYNAMICS AND ENERGY CONVERSION*

Prof. G. A. Brown
Prof. E. N. Carabateas
Prof. R. S. Cooper
Prof. S. I. Freedman
Prof. W. H. Heiser
Prof. M. A. Hoffman
Prof. W. D. Jackson
Prof. J. L. Kerrebrock
Prof. J. E. McCune
Prof. H. P. Meissner
Prof. G. C. Oates
Prof. J. P. Penhune
Prof. J. M. Reynolds III
Prof. A. H. Shapiro
Prof. J. L. Smith, Jr.
Prof. R. E. Stickney
Dr. G. O. Barnett

M. T. Badrawi
J. F. Carson
A. N. Chandra
R. Dethlefsen
D. A. East
R. K. Edwards
J. R. Ellis, Jr.
J. W. Gadzuk
J. B. Heywood
P. G. Katona
G. B. Kliman
A. G. F. Kniazzeh
M. F. Koskinen
K. S. Lee
R. F. Lercari
W. H. Levison

F. C. Lowell, Jr.
B. T. Lubin
S. A. Okereke
J. H. Olsen
E. S. Pierson
R. K. Pollak
R. P. Porter
D. H. Pruslin
C. W. Rook, Jr.
A. W. Rowe
A. Shavit
A. Solbes
R. J. Thome
L. D. Turner
W. F. Ulvang
R. G. Vanderweil
J. C. Wissmiller

A. FREE-SURFACE WAVES MODIFIED BY A MAGNETIC FIELD

A magnetic field tangential to the free surface of a conducting fluid has a substantial effect on the nature of the propagation of small disturbances on that surface. Consider the geometry shown in Fig. X-1. An infinitely deep, incompressible, and inviscid fluid

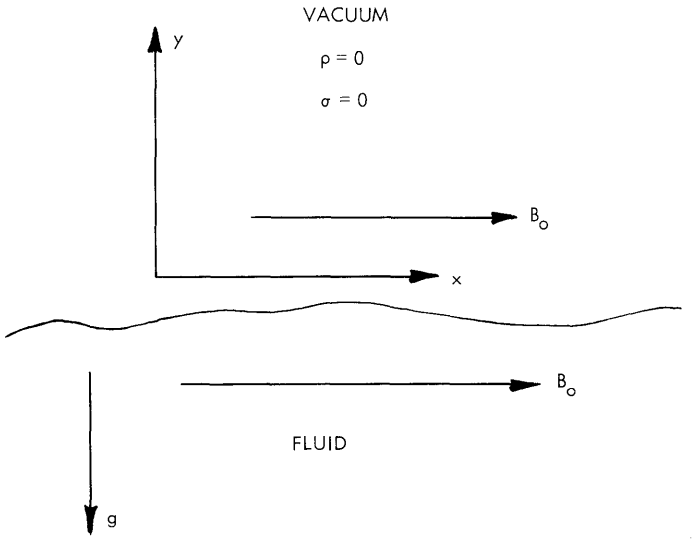

Fig. X-1. Free-surface wave geometry.

*This work was supported in part by the U. S. Air Force (Aeronautical Systems Division) under Contract AF33 (615)-1083 with the Air Force Aero Propulsion Laboratory, Wright-Patterson Air Force Base, Ohio; and in part by the National Science Foundation (Grant G-24073).

with density ρ and electrical conductivity σ has a free surface at the plane $y = 0$. There is a magnetic field in the x direction, and gravitational acceleration acts in the negative y direction. The nonlinear equations of fluid dynamics are linearized to treat small disturbances of the surface.

This problem without a magnetic field is an old one in hydrodynamics. An excellent summary of the work may be found in Stoker.[1] A treatment of the closely related problem with a vertical magnetic field may be found in the paper by Roberts and Boardman.[2] A study of this geometry in which the fluids are assumed to have zero electrical resistivity appears in Chandrasekhar.[3]

Since the wave motion is described by linearized equations, we may, without loss of generality, consider two-dimensional wave motion in the x-y plane with derivatives with respect to z being zero. It is a relatively simple matter to show that the component of magnetic field that is perpendicular to the direction of wave propagation does not affect the motion; hence, we may assume that the applied magnetic field is aligned along the x axis.

1. Equations Describing the Fluid Motion

The equations necessary to describe the motion of the fluid are the linearized inviscid Navier-Stokes equation and Maxwell's equations in the magnetohydrodynamic or quasi-static approximation.

$$\frac{\partial}{\partial t}\bar{v} = -\frac{1}{\rho}\nabla p + (\bar{j}\times\bar{B}_o) \tag{1}$$

$$\bar{j} = \sigma(\bar{E}+\bar{v}\times\bar{B}_o) \tag{2}$$

$$\nabla\times\bar{b} = \mu_o j \tag{3}$$

$$\nabla\times E = -\frac{\partial\bar{b}}{\partial t} \tag{4}$$

$$\nabla\cdot\bar{v} = 0 \tag{5}$$

$$\nabla\cdot\bar{b} = 0. \tag{6}$$

Since the motion is assumed to be two-dimensional in the x-y plane, we may introduce stream functions ψ and A for the velocity and magnetic field.

$$\bar{v} = \psi_y\bar{i}_x - \psi_x\bar{i}_y \tag{7}$$

$$\bar{b} = A_y\bar{i}_x - A_x\bar{i}_y. \tag{8}$$

Substituting these expressions in Eqs. 1-6, we obtain, after a bit of manipulation,

$$\psi_{(xx+yy)t} = \frac{B_o}{\rho\mu_o}A_{(xx+yy)x} \tag{9}$$

$$A_{(xx+yy)} - \sigma\mu_o A_t = -\sigma\mu_o B_o \psi_x. \tag{10}$$

Under the assumption that all quantities are of the form $f(y)\, e^{j(kx-\omega t)}$, this pair of equations can be solved to yield

$$\psi = \left[\psi_1 e^{ky} + \psi_2 e^{\beta y}\right] e^{j(kx-\omega t)} \tag{11}$$

$$A = -\frac{kB_o}{\omega}\left[\psi_1 e^{ky} + M_A^2 \psi_2 e^{\beta y}\right] e^{j(kx-\omega t)}, \tag{12}$$

where

$$M_A^2 = \frac{\omega^2 \rho\mu_o}{k^2 B_o^2} \tag{13}$$

and

$$\beta = k\left[1 - \frac{j\omega\beta\mu_o}{k^2}\left(1 - \frac{k^2 B_o^2}{\omega^2 \mu_o}\right)\right]^{1/2}, \tag{14}$$

Here, the square root with the positive real part is the one intended.

2. Boundary Conditions

The boundary conditions applicable at the free surface are that both components of the magnetic field are continuous and that there is no discontinuity in pressure at the surface. Application of these conditions to the form of solution indicated in Eqs. 11 and 12 gives a dispersion relation between k and ω.

$$\left(1 + \frac{\beta}{k}\right)\frac{\omega^2}{k^2 v_A^2}\left(\omega^2 - gk\right) - 2\left(\frac{\beta}{k}\omega^2 - gk\right) = 0, \tag{15}$$

where

$$v_A^2 = \frac{B_o^2}{\rho\mu_o} \tag{16}$$

and β is defined in Eq. 14.

In the limit as σ goes to zero, the dispersion relation takes the form

$$\frac{\omega^2}{k^2} = \frac{g}{k}. \tag{17}$$

This is the well-known result for gravity waves.

In the limit as the resistivity becomes zero, β approaches infinity in magnitude. The terms depending on $\exp(\beta y)$ are then only of significance near the free surface. This boundary layer contains a high current density that is represented in the perfect conductivity approximation by a surface current. The dispersion relation takes the form

$$\frac{\omega^2}{k^2} = \frac{g}{k} + 2v_A^2. \tag{18}$$

This is the solution that is obtained directly if the fluid is assumed to be perfectly conducting. It is interesting to note here that if the applied magnetic field has a component that is perpendicular to the equilibrium surface of the fluid, no surface current is formed and no simple normal-mode dispersion relation exists.

There are two spurious solutions to Eqs. 14 and 15. They are

$$\omega^2 = k^2 v_A^2. \tag{19}$$

3. The Effects of Small Losses

Equations 17 and 18 represent the two lossless limits of the situation under consideration. We now consider the effects of small loss on these limiting forms. It is convenient to introduce dimensionless variables. A useful choice of characteristic dimensions is

$$L = \frac{v_A^2}{g}$$

$$T = \frac{v_A}{g}.$$

The dimensionless variables will be

$$\omega' = T\omega$$

$$k' = Lk$$

$$\beta' = \beta/k.$$

Equations 14 and 15 become

$$\beta^1 = \left[1 - jR_M \frac{\omega^1}{k'^2}\left(1 - \frac{k'^2}{\omega'^2}\right)\right]^{1/2} \tag{20}$$

$$\frac{\omega'^2}{k'^2}(\omega'^2 - k)(1+\beta') - 2(\beta'\omega'^2 - k'), \tag{21}$$

where R_M is a magnetic Reynolds number

$$R_M = \frac{\sigma\mu_o v_A^3}{g}. \tag{22}$$

To explore effects of small conductivity, we can write ω as a power series in the magnetic Reynolds number.

$$\omega' = \omega'_o + R_M \omega'_1 + R_M^2 \omega'_2 + \ldots .$$

When this is done, we find

$$\omega'_o = k^{1/2}$$

$$\omega'_1 = -j/4$$

$$\omega'_2 = \frac{4 - 7\omega'^2_o}{32\omega'^3_o}.$$

Two peculiar features may be noted. First, the rate of damping is independent of wavelength. Second, the rate of oscillation of the system may either increase or decrease with the addition of small loss, the change depending upon the wavelength.

For large conductivity, an appropriate expansion parameter is

$$\gamma = \frac{1}{R_M^{1/2}}.$$

Writing

$$\omega' = \omega'_o + \gamma\omega'_1 + \gamma^2\omega'_2 + \ldots ,$$

we find

$$\omega_o = [k(1+2k)]^{1/2}$$

$$\omega_1 = -2\left[\frac{jk^2}{\omega_o k(1+k)}\right]^{1/2} \frac{2k^2(1+k)}{1+2k}.$$

The general dispersion relation has a number of interesting features, and it is being investigated numerically.

C. W. Rook, Jr.

References

1. J. J. Stoker, Water Waves (Interscience Publishers, New York, 1957).

2. P. Roberts and A. Boardman, Astrophys. J. 135, 552 (1962).

3. S. Chandrasekhar, Hydrodynamics and Hydromagnetic Stability (Oxford University Press, London, 1961), pp. 457-465.

B. EFFECT OF SOME IMPERFECTIONS ON LIQUID-METAL HYDROMAGNETIC WAVEGUIDE PERFORMANCE

In the analysis of hydromagnetic waveguides, the effects of viscosity, fringing fields, and finite conductivity walls are usually neglected. An example of each factor will be given separately and in infinite plane parallel geometry for simplicity. The waveguide geometry is given in Fig. X-2.

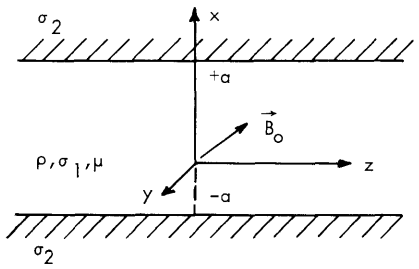

Fig. X-2. Waveguide geometry $\frac{\partial}{\partial y} = 0$.

The waveguide is formed by two semi-infinite regions of conductivity σ_2 spaced a distance 2a apart with faces parallel to the y-z plane. The fluid between the planes has density ρ, conductivity σ_1, and absolute viscosity μ. The imposed uniform DC magnetic field is given by

$$\vec{B}_o = \vec{i}_x B_{ox} + \vec{i}_z B_{oz}. \tag{1}$$

The wave will be assumed to be TM (principal mode) and varying as

$$A(x, z, t) = a(x)\, e^{i(\omega t + kz)}. \tag{2}$$

The relevant equations in the fluid may now be written as

$$i\omega\rho v_y = -j_x B_{oz} + j_z B_{ox} - \mu k^2 v_y + \mu \frac{d^2 v_y}{dx^2} \qquad \text{Navier-Stokes} \tag{3}$$

$$\left.\begin{aligned} j_x &= \sigma_1(e_x + v_y B_{oz}) \\ j_z &= \sigma_1(e_z - v_y B_{ox}) \end{aligned}\right\} \quad \text{Ohm's Law} \tag{4, 5}$$

$$ike_x - \frac{de_z}{dx} = -i\omega b_y \qquad \text{curl } \vec{e} \tag{6}$$

$$\left.\begin{aligned} -ikb_y &= \mu_o j_x \\ \frac{db_y}{dx} &= \mu_o j_z \end{aligned}\right\} \quad \text{curl } \vec{b} \tag{7, 8}$$

1. The Effect of Viscosity $B_{ox} = 0$

Equations 3-8 may now be reduced to a single fourth-order equation in v_y.

$$\nu\eta \frac{d^4 v_y}{dx^4} - \left[\eta(k^2\nu + i\omega) + \nu(k^2\eta + i\omega)\right] \frac{d^2 v_y}{dx^2} + \left[(k^2\nu + i\omega)(k^2\eta + i\omega) + k^2 c_{oz}^2\right] v_y = 0, \tag{9}$$

where

$$\nu = \frac{\mu}{\rho} = \text{viscous diffusivity} \tag{10}$$

$$\eta = \frac{1}{\mu_o \sigma_1} = \text{magnetic diffusivity} \tag{11}$$

$$c_{oz} = \frac{B_{oz}}{\sqrt{\mu_o \rho}} = \text{longitudinal Alfvén speed.} \tag{12}$$

Note the symmetry of the magnetic and viscous diffusivities in (9).

The solution of Eq. 9 has been investigated by Blue[1] for $\sigma_2 = 0$. In this case, the electromagnetic boundary condition requires the velocity to be zero at the walls quite independently of viscosity. He found that for liquid metals visocity played no significant part. For a perfectly conducting wall $\sigma_2 = \infty$, however, the electromagnetic boundary condition requires a velocity that is maximum at the walls if $\mu = 0$. Viscosity might then be expected to have a significant effect.

The antisymmetric solution of (9) is

$$v_y = A_1 \sin \gamma_1 x + A_2 \sinh \gamma_2 x. \tag{13}$$

The boundary conditions for $\sigma_2 = \infty$ are

$$v_y(a) = 0 \tag{14}$$

$$e_z(a) = 0, \tag{15}$$

where

$$e_z = -\frac{\eta B_o}{ikc_{oz}^2}\left[\nu\frac{d^3v_y}{dx^3} - (k^2\nu+i\omega)\frac{dv_y}{dx}\right] \tag{16}$$

and

$$\gamma^2 = -(k^2+i\omega)\frac{\nu+\eta}{2\nu\eta} \pm \sqrt{\left(i\omega\frac{\nu-\eta}{2\nu\eta}\right)^2 - \frac{k^2c_{oz}^2}{\nu\eta}}\,. \tag{17}$$

Here, γ_1 is associated with the + sign and γ_2 with the - sign.

Since in a typical liquid metal (NaK) at room temperature $\nu = 9.7\times10^{-8}$ m^2/s and $\eta = 0.3$ m^2/s, take the limiting forms of γ_1 and γ_2 as $\nu \to 0$

$$\gamma_1^2 = \frac{\omega^2 - k^2\left(c_{oz}^2+i\omega\eta\right)}{i\omega\eta} \tag{18}$$

$$\gamma_2^2 = -\frac{i\omega}{\nu}. \tag{19}$$

Notice that γ_1^2 is just that which would have been obtained if viscosity had been neglected at the outset. The velocity and tangential field then become

$$v_y = A_1\left[\sin\gamma_1 x - 2e^{-(1-i)\sqrt{\frac{\omega}{2\nu}}(a-x)}\right] \tag{20}$$

$$e_z = A_1\frac{\omega\eta B_o}{kc_{oz}^2}\cos\gamma_1 x. \tag{21}$$

The effect of the second term in (20) decays away from the wall with a characteristic distance

$$\delta = \sqrt{\frac{2\nu}{\omega}} = \text{viscous skin depth.} \tag{22}$$

In NaK at $\omega = 400$ (a frequency near the lower end of the Alfvén region[2]) $\delta = 0.002$ cm and decreases with increasing frequency. Summarizing these results, we see that the effect of viscosity is only to introduce a thin boundary layer near the wall in the velocity and does not affect the tangential electric field, as illustrated in Fig. X-3, in which the relative thickness of the boundary layer has been exaggerated.

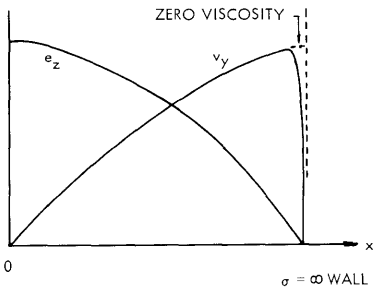

Fig. X-3. Effect of viscosity on e_z and v_y.

2. Effect of Finite Wall Conductivity $B_{ox} = \mu = 0$ for $\eta_1 = \eta$

In this case the fields in the fluid are given by setting $\nu = 0$, and are

$$b_{y1} = A_1 \sin \gamma_1 x \tag{23}$$

$$e_{z1} = A_1 \eta_1 \gamma_1 \cos \gamma_1 x, \tag{24}$$

where γ_1 is given by (18). In the walls

$$b_{y2} = A_2 e^{-\gamma_3 x} \tag{25}$$

$$e_{z2} = -A_2 \eta_2 \gamma_3 e^{-\gamma_3 x}, \tag{26}$$

where

$$\eta_2 = \frac{1}{\mu_o \sigma_2} \tag{27}$$

and

$$\gamma_3^2 = -\frac{\omega^2 - i\omega\eta_2 k^2}{i\omega\eta_2}. \tag{28}$$

Setting the tangential electric and magnetic fields equal at the walls yields

$$\tan \gamma_1 a = -\frac{\sigma_2}{\sigma_1}\frac{\gamma_1}{\gamma_3}. \tag{29}$$

It is evident that γ_1 and γ_3 must now be complex, thereby making the solution of (29) for k^2 quite difficult. Approximate solutions may be obtained for σ_2 very large and very small, but are not very useful.

If the wall is assumed to be of finite thickness b much less than an electromagnetic skin depth so that the wall current may be considered constant in x, then (29) becomes

$$\tan \gamma_1 a = -\frac{\sigma_2}{\sigma_1} \frac{b}{a} \gamma_1 a. \tag{30}$$

This assumption will be good for b = 0.25 inch and frequencies in the NaK-Alfvén region for stainless-steel and even for copper walls. Equation 30 may be solved graphically as in Fig. X-4 for γ_1 and thus k.

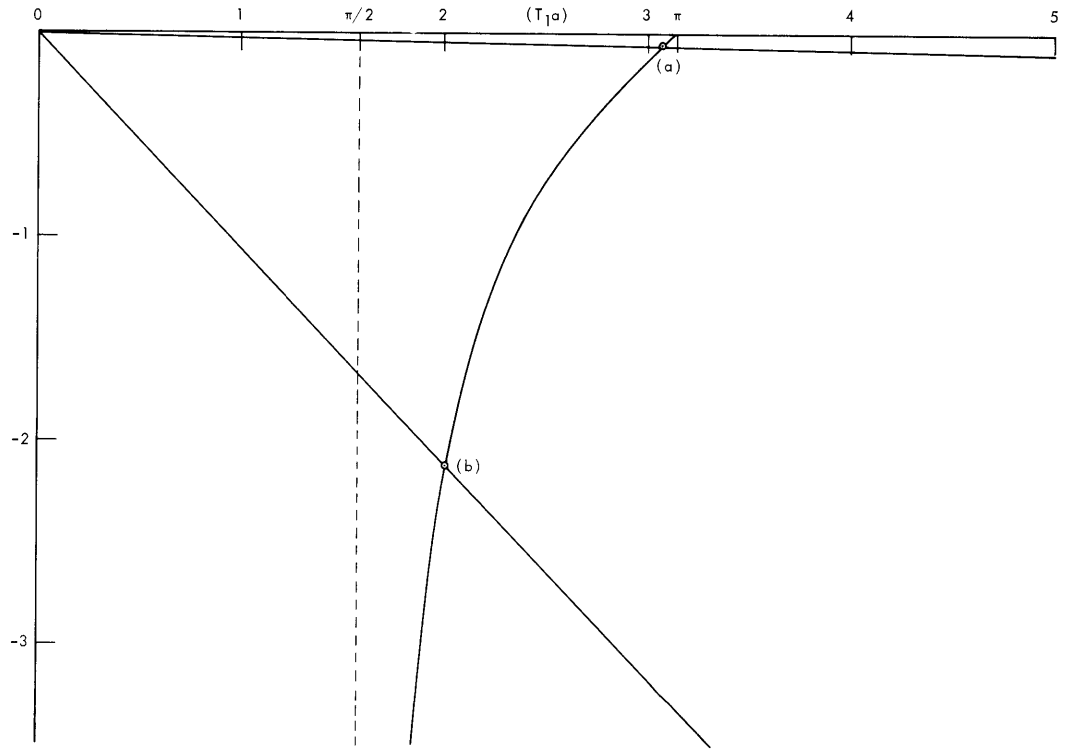

Fig. X-4. Graphical solution of Eq. 30 for NaK with
(a) stainless-steel wall, a = 7.5 in., b = 0.25 in.;
(b) copper wall, a = 6 in., b = 0.25 in.

Notice in Fig. X-4 that an NaK waveguide constructed of stainless steel (even if good electrical contact could be made) is almost equivalent to a perfect insulator, while copper approaches reasonably close to being a perfect conductor.

3. Effect of Fringing Fields $\mu = 0$

After some reduction, Eqs. 3-8 become

$$-\left(c_o^2+i\omega\eta_1\right) ik\eta_1 b_y = \left(c_{ox}^2+i\omega\eta_1\right)e_x + c_{ox}c_{oz}e_z \tag{31}$$

$$\left(c_o^2+i\omega\eta_1\right)\eta_1 \frac{db_y}{dx} = c_{ox}c_{oz}e_x + \left(c_{oz}^2+i\omega\eta_1\right)e_z, \tag{32}$$

where

$$c_{ox} = \frac{B_{ox}}{\sqrt{\mu_o\rho}} = \text{transverse Alfvén speed} \tag{33}$$

$$c_o^2 = c_{ox}^2 + c_{oz}^2. \tag{34}$$

Equations 31 and 32 may now be combined to give

$$\left(c_{ox}^2+i\omega\eta_1\right)\frac{d^2b_y}{dx^2} + 2ikc_{ox}c_{oz}\frac{db_y}{dx} + \left[\omega^2-k^2\left(c_{oz}^2+i\omega\eta_1\right)\right]b_y = 0 \tag{35}$$

$$e_z = \frac{1}{i\omega}\left[\left(c_{ox}^2+i\omega\eta_1\right)\frac{db_y}{dx} + ikc_{ox}c_{oz}b_y\right]. \tag{36}$$

The antisymmetric solution of 35 is

$$b_y = A_1 e^{-iT_1x}\sin T_2x \tag{37}$$

$$e_z = A_1\frac{T_2\left(c_{ox}^2+i\omega\eta_1\right)}{i\omega}e^{-T_1x}\cos T_2x, \tag{38}$$

where

$$T_1 = \frac{kc_{ox}c_{oz}}{c_{ox}^2 + i\omega\eta_1} \tag{39}$$

and

$$T_2 = \frac{1}{c_{ox}^2 + i\omega\eta_1}\left[\omega^2\left(c_{ox}^2+i\omega\eta_1\right) - i\omega\eta_1k^2\left(c_o^2+i\omega\eta_1\right)\right]^{1/2}. \tag{40}$$

Application of the boundary condition either for an insulated wall $b_y(a) = 0$ or for an infinite conductivity wall $e_z(a) = 0$ fixes T_2 and thus k^2.

$$k^2 = \left(\frac{\omega}{c_{oz}}\right)^2\frac{1+\frac{2\omega_1}{i\omega}+\frac{2\omega_1}{i\omega}\frac{2\omega_2}{i\omega}}{1+\frac{i\omega}{2\omega_2}+\delta^2}\left(1+\frac{2\omega_2}{i\omega}\delta^2\right), \tag{41}$$

where ω_1 and ω_2 are the critical frequencies[2]

$$\omega_1 = \frac{1}{2}\eta_1 T_2^2 \tag{42}$$

$$\omega_2 = \frac{1}{2}\frac{c_{oz}^2}{\eta_1} \tag{43}$$

and

$$\delta = \frac{c_{ox}}{c_{oz}}. \tag{44}$$

An exact evaluation of (44) is shown in Fig. X-5 (log-log coordinates) for an NaK experiment, $\delta = 0.1$, with the curve for $\delta = 0$ dashed for comparison. Notice that the

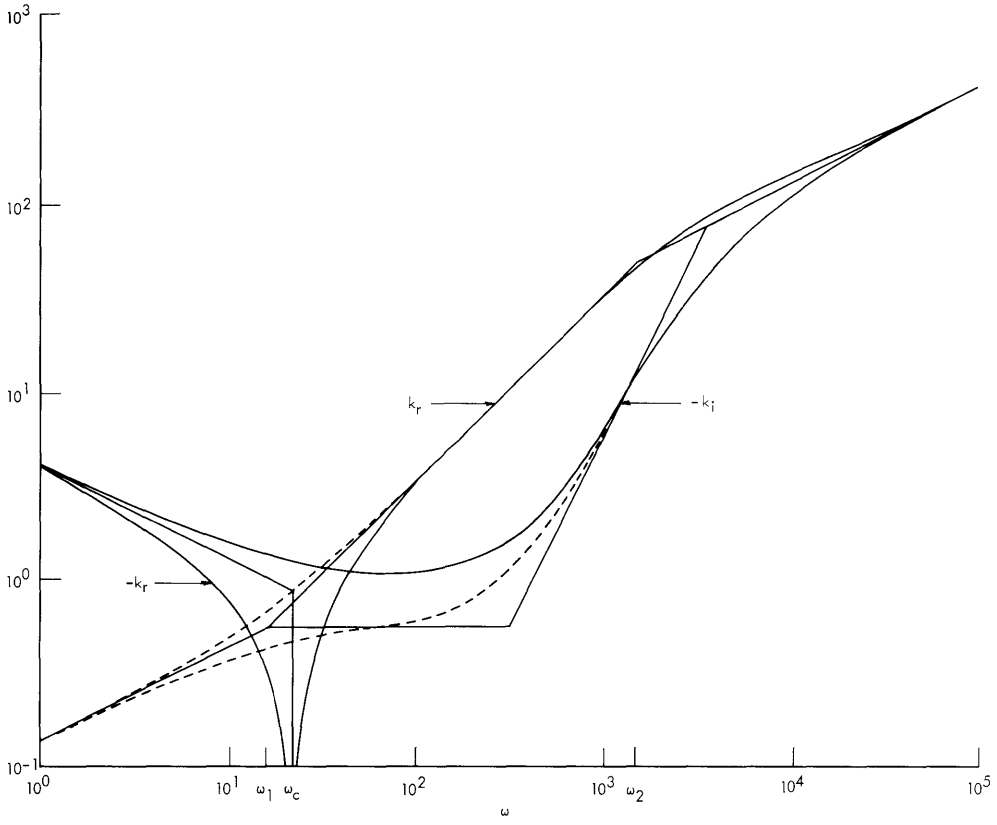

Fig. X-5. Propagation constant with transverse field effect in NaK. (B_{oz} = 8 kgauss; a = 6 in.; $\delta = 0.1$; $\sigma_2 = \infty$.)

real part of k goes to zero at the frequency ω_c. If $\delta < 1$, this frequency is given by

$$\omega_c = \frac{2\omega_2\delta^2}{\sqrt{1+\frac{\omega_2}{\omega_1}\delta^2}}, \tag{45}$$

and is due to an ordinary cutoff in the transverse field. As the transverse field component is made smaller, $\delta \to 0$, this cutoff recedes to zero frequency.

G. B. Kliman

References

1. E. Blue, Torsional MHD Waves in the Presence of Finite Viscosity, AFOSR TN-57-57, January 1957.

2. G. B. Kliman, Some properties of magnetohydrodynamic waveguides, Quarterly Progress Report No. 72, Research Laboratory of Electronics, M. I. T., January 15, 1964, pp. 144-149.

C. FRICTION-FACTOR MEASUREMENTS IN LIQUID-METAL MAGNETOHYDRODYNAMIC CHANNEL FLOWS

Pressure-flow relations in a constant, transverse magnetic field region provide information on the character of MHD channel flows and the energy conversion devices based on these flows.[1] Data on friction factors in such a uniform field region of a constant-area channel have been obtained for NaK flows by using the flow facility described in Quarterly Progress Report No. 72 (pages 156-163).

Table X-1. Comparative maxima for important parameters.

Investigator	R	M/R_{max}	M^2/R_{max}
Hartmann and Lazarus[2]	4.9×10^3	1.5×10^{-3}	1.1×10^{-2}
	3.2×10^3	1.9×10^{-3}	1.4×10^{-2}
Murgatroyd[3]	7×10^4	1.8×10^{-3}	2.2×10^{-1}
	3×10^4	2.1×10^{-3}	1.3×10^{-1}
Brouillette and Lykoudis[5]	7.7×10^4	2.3×10^{-4}	4.0×10^{-3}
	4.0×10^5	4.5×10^{-5}	8.1×10^{-4}
Present	6.0×10^4	1.1×10^{-3}	7.2×10^{-2}
	3.2×10^4	2.5×10^{-3}	2.0×10^{-1}

Previous experimental work in this area has employed mercury.[2-5] Sodium potassium gives much larger values of Hartmann number (M) for a given channel and magnetic field, and thus much larger ranges of M/R and M^2/R, where R is the Reynolds number. Comparative maxima are given in Table X-1. The higher values attained by Murgatroyd[3] are due to his much higher field strength (20,000 gauss as opposed to 5500 for the present work).

The channel is shown schematically in Fig. X-6, in which B_o and U_o are the applied magnetic field and mean velocity, respectively. Magnetic flux density, continuously variable up to a value of 5500 gauss and virtually uniform over the channel section of interest, was supplied by an electromagnet. Flow was provided by a 20-gal/min, 20-psi positive displacement pump, and surge tanks ensured that it was almost pulsation-free.

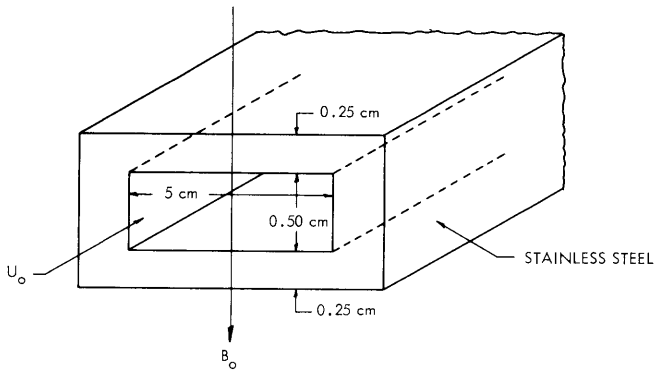

Fig. X-6. Channel cross section.

Pressure differences were read directly from NaK manometers, with a small amount of kerosene on top of each to improve readability. Velocity was measured by a calibrated Venturi meter, whose pressure differences were read as indicated above. Fluid temperature was read by a thermocouple potentiometer unit. Voltages across the channel and an electromagnetic flowmeter in the loop were obtained by using a high-impedance oscilloscope.

The results of pressure measurements are shown as friction factors vs M/R in Figs. X-7 and X-8. The friction factor is defined as

$$h_L = f \frac{U_o^2}{2g} \frac{L}{D}, \tag{1}$$

where h_L is the hydraulic head loss along a length L of a uniform channel of hydraulic radius D in which fluid is flowing with mean velocity U_o, and g is the gravitational

constant.

It is well established that liquid metals generally do not wet solid metal surfaces.[6,7] Under such circumstances very poor electrical contact exists. It is thus reasonable to assume that the walls of the channel make poor electrical contact with the fluid. The

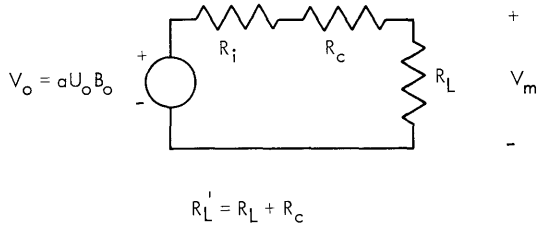

Fig. X-7. Lumped-circuit model of nonwetting contact.

voltages measured across the channel were approximately 5 per cent of those predicted and measured[8] for insulated side walls and highly conducting end walls and thus confirmed the existence of an electrical contact resistance, R_c, substantially greater than the channel internal resistance R_i.

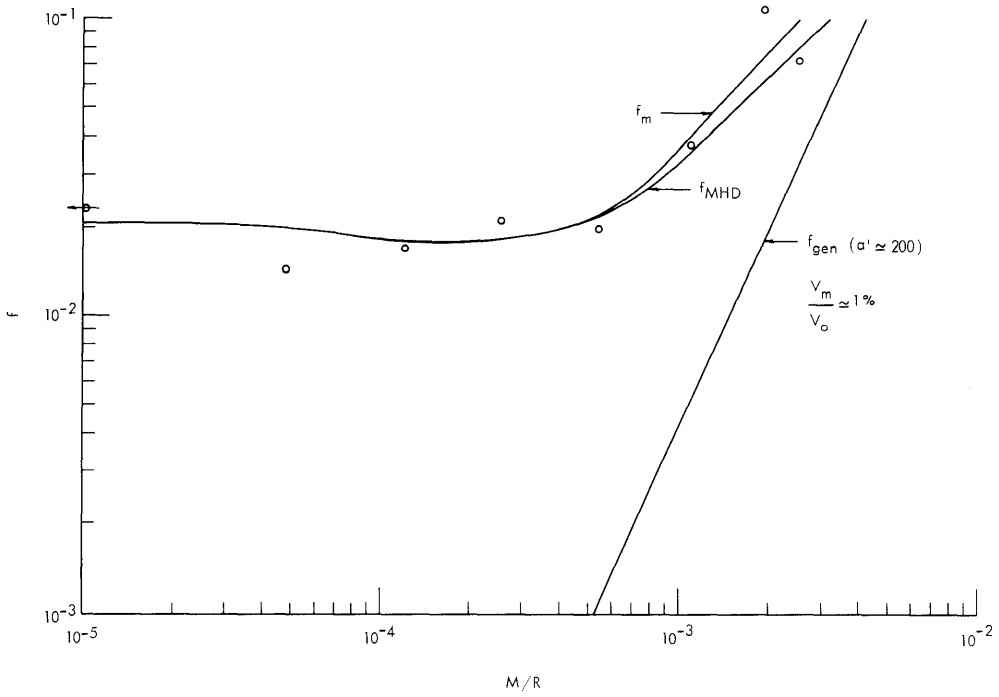

Fig. X-8. Friction factor vs M/R for $R \approx 3.2 \times 10^4$.

A circuit representation of the situation is shown in Fig. X-7, in which R_L is the load imposed by the finite conductivity walls and V_o is the open-circuit voltage. From a one-dimensional treatment,

$$V_o = aU_oB_o, \tag{2}$$

where a is the interelectrode distance, U_o is the mean flow velocity for either turbulent or laminar flow, and B_o is the uniform applied magnetic field.

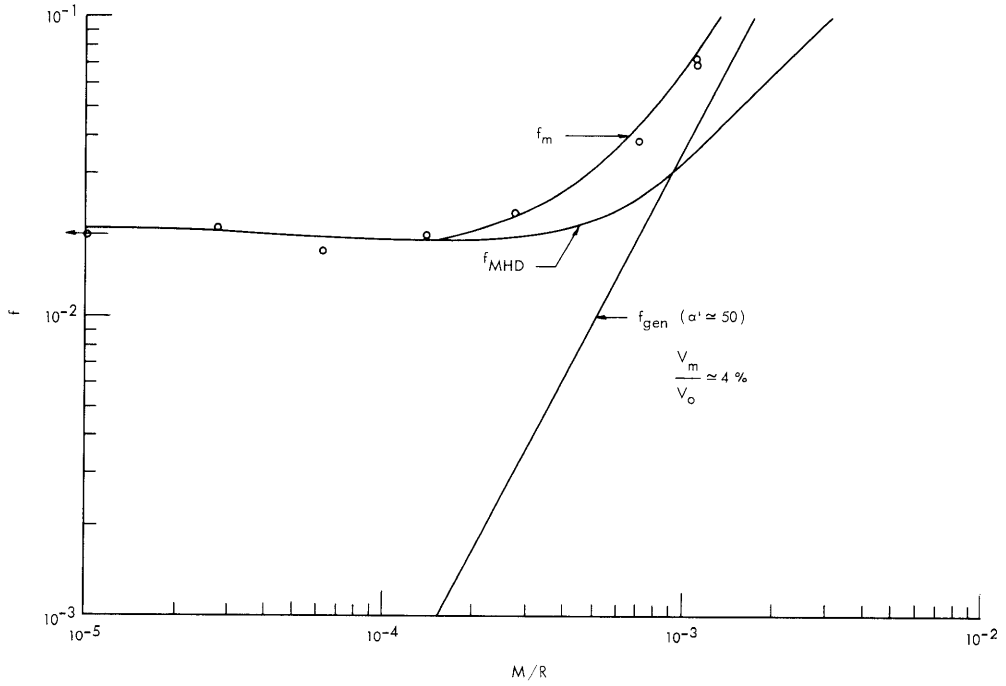

Fig. X-9. Friction factor vs M/R for $R \approx 6 \times 10^4$.

It is convenient to define a resistance ratio a' as

$$a' = \frac{R_L + R_c}{R_i}, \tag{3}$$

where a' is determined from measured voltage V_m, since

$$\frac{V_m}{V_o} = \frac{R_L}{R_L + R_i + R_c} = \frac{R_L/R_i}{1 + a'}. \tag{4}$$

By rewriting the result of Penhune[9] for laminar flow, the equivalent friction factor f_m is

$$f_m = \frac{32M^2}{R} \frac{(a' + M \coth M)}{(a'+1)(M \coth M - 1)}. \quad (5)$$

For turbulent flow, a similar result holds,

$$f_m = \frac{32M^2}{a'R} + f_{mhd}, \quad (6)$$

where f_{mhd} denotes the insulated-wall MHD friction factor obtained by Murgatroyd.[3] In Eqs. 5 and 6

$$R = \frac{\rho U_o D}{\eta}, \quad \text{and} \quad M^2 = B_o^2 \left(\frac{D}{4}\right)^2 \frac{\sigma}{\eta},$$

where ρ is the density, η is the viscosity, and σ is the conductivity of the fluid.

In this study $a' \geq 50$, and the two expressions differ by less than 5 per cent in regions for which both apply.

Equation 6 is plotted in Figs. X-8 and X-9 for comparison with observed values, and shows good agreement over the entire range of M/R values. Work is now in progress to obtain data over a wider range of channel and electrical loading conditions. Copper electrodes will be used to ensure wetting contacts.

W. D. Jackson, J. R. Ellis, Jr.

References

1. L. P. Harris, Hydromagnetic Channel Flows (The Technology Press of Massachusetts Institute of Technology, Cambridge, Mass., and John Wiley and Sons, Inc., New York, 1960).

2. J. Hartmann and F. Lazarus, Hg dynamics. II, Det. Kgl. Danske Vidensk. Selskab Matt.-Fys. Medd., Vol. 15, No. 7, 1937.

3. W. Murgatroyd, Experiments on magnetohydrodynamic channel flow, Phil. Mag. 44, 1348 (1953).

4. H. Branover and O. Lielausis, Effect of Transverse Magnetic Field on Internal Structure and Hydraulic Resistance in Turbulent Flows of Liquid Metals, Latvijas P. S. R. Zin. Akad. Vestis, 1 (162), 59 (1961).

5. E. C. Brouillette and P. S. Lykoudis, Measurements of Skin Friction for Turbulent Magneto-fluid Mechanic Channel Flow, Research Project No. 3093, Purdue Research Foundation, August 1962.

6. N. K. Adam, Physics and Chemistry of Surfaces (Oxford University Press, London, 1941).

7. A. Bondi, Spreading of liquid metals on solid surfaces, Chem. Rev. 52, 417 (1953).

8. W. D. Jackson, Measurement of motionally induced voltage in some magnetohydrodynamic channel flows, Bull. Am. Phys. Soc. 9, 208 (1961).

9. J. P. Penhune, Energy Conversion in Laminar Magnetohydrodynamic Channel Flow, ASD TR 61-294, Research Laboratory of Electronics, M. I. T., August 1961.

D. DIPOLE-DIPOLE INTERACTIONS BETWEEN A POLARIZABLE PARTICLE AND AN ADSORBED LAYER OF DISCRETE DIPOLES

1. Introduction

This is the second in a series of reports that will present the results of analytical studies of cesium films adsorbed on refractory metal substrates. Since a cesium film of less than one monolayer adsorbed on materials such as tungsten serves to reduce the work function of the surface, adsorption phenomena are pertinent to thermionics research. Analytical results have been presented in previous works[1-3] relating atomic and ionic heats of adsorption and electron work function to the degree of coverage. These results compare favorably with available experimental data.[4,5]

The initial phase of this research has already been presented.[6] Two values for the penetration coefficient, one for a mobile film, and one for an immobile film, were derived. The experimental values fell between the two. In the treatment presented in the first report an important effect was not considered – the effect of polarization of the adsorbed particles while they are in the strong depolarizing field of the other ions.[7] A method for calculating the effect of the depolarizing field of the discrete dipole layer on a given test particle is presented in this report which is based on the adsorption model given previously.[6]

If an ion is placed in the depolarizing field that results from an adsorbed layer of discrete dipoles, the field will induce a dipole moment in the test particle, directed toward the surface, by distorting the charge distribution of the electron cloud. This moment is given by

$$\mu_i = \alpha E, \tag{1}$$

where α is the polarizability of the test particle. The interaction of the induced dipole with the discrete dipoles will be repulsive. The object of this report is to derive an approximate analytical expression to describe this repulsive dipole-dipole interaction as a function of the distance of the test particle from the dipole layer.

2. Depolarizing Field

The induced dipole given by Eq. 1 can be determined by knowing the depolarizing field. An approximate field can be obtained by the following method. The potential at the charge center of an adsorbed ion in the dipole layer as determined previously[8] is equal to $V(r=\lambda) = \dfrac{2.25q\theta_i^{3/2}\lambda^2}{d^3}$. It can be shown that for r of the order of λ the relation

$$V(r) = \frac{2.25q\lambda\theta_i^{3/2}r}{d^3} \tag{2}$$

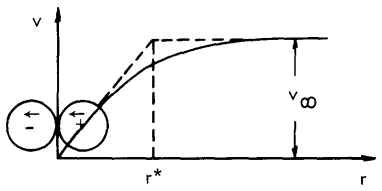

Fig. X-10. Adsorbed dipole layer potential as a function of distance from the substrate.

is also valid. As r becomes large, $V(r) \rightarrow V_\infty = 2\pi M\sigma_1\theta$. The description of $V = V(r)$ between the region in which the linear approximation is no longer valid and the region in which r approaches infinity has been derived but is extremely complicated to evaluate in a simple manner. The relation is of such a form that little accuracy is lost by making the following linearizing assumption. Consider the potential to increase linearly by Eq. 2 until $V(r) = V_\infty$ at r^* as shown in Fig. X-10. Setting $V(r) = V_\infty$ and solving for $r = r^*$ yield

$$r^* = \frac{\pi d}{2.25\theta_i^{1/2}}. \tag{3}$$

The linearized potential is equivalent to a region for $r \leq r^*$ in which the depolarizing field is constant and given by

$$E = \frac{\partial V(r)}{\partial r} = \frac{2.25q\lambda\theta_i^{3/2}}{d^3} \tag{4}$$

and a field-free region for $r > r^*$.

3. Analysis

Since the difference in potential of an ion at infinity and an $r < r^*$ is desired, consider the process of bringing an ion from infinity to $r < r^*$. As the ion moves from infinity to r^*, the only interaction is that of a positively charged particle with a dipole layer.[6] At $r = r^*$, the ion enters the depolarizing field, at which point a moment is induced in the ion $\mu_i = \alpha E$. As the ion approaches the surface from r^* there are two types of interactions to consider, that of the positive charge with the adsorbates and that of the induced dipole with the discrete dipoles at each adsorption site. The potential resulting from the dipole-dipole interaction of the induced dipole of the test particle with the dipoles of the adsorbed layer at the lattice site identified by the indices i, j is given by[9, 10]

$$qV_{ij} = \frac{\vec{M}_{ij} \cdot \vec{\mu}_i - 3(\vec{n} \cdot \vec{M}_{ij})(\vec{n} \cdot \vec{\mu}_i)}{r_{ij}^3}, \tag{5}$$

where

$$M_{ij} = q\lambda - aE \tag{6}$$

and r_{ij} is identified in Fig. XVII-21 of Quarterly Progress Report No. 72 (page 167), $\vec{n}$ is a unit vector along r_{ij}, and M_{ij} is considered as a point dipole at i, j with r = 0. Since M_{ij} and μ_i are parallel, Eq. 5 becomes

$$qV_{ij} = -\frac{M_{ij}\mu_i(1-3\cos^2\theta_{ij})}{r_{ij}^3}, \tag{7}$$

where

$$r_{ij}^2 = \frac{4d^2}{\theta_i}(i^2+j^2) \tag{8a}$$

$$\cos^2\theta_{ij} = \frac{r^2}{r_{ij}^2}. \tag{8b}$$

Combining Eqs. 7 and 8 yields

$$qV_{ij}(r) = -\frac{M_{ij}\mu_i\theta_i^{3/2}}{8d^3}\left[\frac{1}{(i^2+j^2)^{3/2}} - \frac{3r^2\theta_i}{4d^2(i^2+j^2)^{5/2}}\right]. \tag{9}$$

Since by definition V = 0 at r = 0, Eq. 9 becomes

$$qV_{ij}(r) = -\frac{3M_{ij}\mu_i\theta_i^{5/2}r^2}{32d^5(i^2+j^2)^{5/2}}$$

and

$$qV(r) = -\frac{3M_{ij}\mu_i\theta_i^{5/2}r^2}{32d^5}\sum_{-\infty}^{\infty}\sum\frac{1}{(i^2+j^2)^{5/2}}. \tag{10}$$

Combining Eqs. 1, 4, 6, and 10 together with $\sum_{-\infty}^{\infty}\sum\frac{1}{(i^2+j^2)^{5/2}} \approx 5.04$ gives for the final result

$$V_i(r) = -\frac{1.06q\lambda^2 a\theta_i^4 r^2}{d^8}\left(1 - \frac{2.25a}{d^3}\theta_i^{3/2}\right) \qquad \text{for } r \leq r^*$$

$$V_i(r) = V_i(r^*) \qquad \text{for } r \geq r^* \tag{11}$$

This is the analytic statement of the potential resulting from induced dipoles.

The change in adsorption properties of ions from depolarization may be determined from Eq. 11. The dipole-dipole interaction of induced dipoles in atomic species with the surface dipoles is much greater than that interaction occurring between induced dipoles in ions and surface dipoles because the polarizability of the cesium atom is almost twenty times as great as that of ions. The expression for the dipole-dipole interaction of an atom passing through the dipole field given by Eq. 4 is

$$V_a(r) = -\frac{1.06q\lambda^2 a_a\theta_i^4 r^2}{d^8}\left(1 - \frac{2.25a_i}{d^3}\theta_i^{3/2}\right) \tag{12}$$

where a_a is the atom polarizability, and a_i is the ion polarizability.

$V_i(r^*)$ and $V_a(r^*)$ are calculated for the cesium-tungsten system and the results presented in Table X-2. The results are for conditions at T = 800° K with λ = 1.65 Å,

Table X-2. Potential across ionic and atomic depolarizing dipole layers.

θ	θ_i	$V_i(r=r^*)$ eV	$V_a(r=r^*)$ eV
0	0	0	0
.05	.05	2.4×10^{-5}	2.48×10^{-4}
.1	.1	1.69×10^{-4}	3.16×10^{-3}
.2	.2	1.32×10^{-3}	2.47×10^{-2}
.3	.3	4.42×10^{-3}	8.25×10^{-2}
.4	.4	1×10^{-2}	.187
.5	.5	1.89×10^{-2}	.354
.6	.586	3×10^{-2}	.561
.7	.666	4.25×10^{-2}	.795
.8	.732	5.5×10^{-2}	1.03
.9	.782	6.53×10^{-2}	1.22
1.0	.85	8.07×10^{-2}	1.51

the cesium ionic core radius; d = 3.15 Å, the tungsten lattice parameter; $\alpha_i = 2.46$ Å^3, $\alpha_a = 46$ Å^3.[11] As is to be expected, the interaction is significant only between the induced moment in the atom and the dipole layer, since this moment is nearly twenty times as great as that which is induced in the ionic species.

The results presented in this analysis will be essential in the continuation of this work on adsorption phenomena of monolayers, since a quantitative means of determining the effects of polarization of atoms and ions and of ions in a dipole field was needed. This is provided by Eqs. 11 and 12. Work is in progress to show the effects of the dipole-dipole interactions on the penetration coefficient, work function, and atomic and ionic heats of adsorption.

J. W. Gadzuk

References

1. N. S. Rasor and C. Warner III, Correlation of emission processes for adsorbed films (to be published in J. Appl. Phys.).

2. E. N. Carabateas, Analytical Description of Cesium Films on Metal, Report to the National Science Foundation, "Basic Studies on Cesium Thermionic Converters," June 1963.

3. J. D. Levine, Adsorption Physics of Metals Partially Coated by Metallic Films, Ph.D. Thesis, Department of Nuclear Engineering, M.I.T., 1963.

4. J. B. Taylor and I. Langmuir, Phys. Rev. 44, 423 (1933).

5. J. M. Houston, Advances In Electronics, Vol 17, p. 147, 1962.

6. J. W. Gadzuk, Penetration of an ion through an ionic dipole layer at an electrodes surface, Quarterly Progress Report No. 72, Research Laboratory of Electronics, M.I.T., January 15, 1964, pp. 166-174.

7. J. H. de Boer and C. F. Veenemans, Physica 1, 953-959 (1934).

8. J. W. Gadzuk, op. cit., Eq. 6.

9. T. H. Berlin and J. S. Thomsen, J. Chem. Phys. 20, 1368 (1952).

10. J. D. Jackson, Classical Electrodynamics (John Wiley and Sons, Inc., New York, 1962), p. 102.

11. J. H. de Boer, Electron Emission and Adsorption Phenomena (Cambridge University Press, London, 1935).